*remote sensing*

MDPI

*Article*

# Phytoplankton Size Structure in Association with Mesoscale Eddies off Central-Southern Chile: The Satellite Application of a Phytoplankton Size-Class Model

**Andrea Corredor-Acosta [1,2], Carmen E. Morales [2,3,*], Robert J. W. Brewin [4,5], Pierre-Amaël Auger [2,6], Oscar Pizarro [2,7,8], Samuel Hormazabal [2,6] and Valeria Anabalón [2,9]**

1 Departament of Oceanography, Faculty of Natural Sciences and Oceanography, University of Concepción, Casilla 160-C, Concepción 4070386, Chile; jcorredor@oceanografia.udec.cl
2 Institute Milenio of Oceanography (IMO), University of Concepción, Concepción 4030000, Chile; pierreamael.auger@gmail.com (P.A.A.); oscar.pizarro@imo-chile.cl (O.P.); samuel.hormazabal@pucv.cl (S.H.); vanabalo@gmail.com (V.A.)
3 Departament dof Oceanography, Faculty of Natural Sciences and Oceanography, University of Concepción, Barrio Universitario s/n, Concepción 4070386, Chile
4 Plymouth Marine Laboratory, Prospect Place, The Hoe, Plymouth PL1 3DH, UK; robr@pml.ac.uk
5 National Centre for Earth Observation, Plymouth Marine Laboratory, Prospect Place, The Hoe, Plymouth PL1 3DH, UK
6 Escuela de Ciencias del Mar, Pontificia Universidad Católica de Valparaíso, Valparaíso 2340000, Chile
7 Departament of Geophysics, Universidad de Concepción, Barrio Universitario s/n, Concepción 4070386, Chile
8 COPAS-Sur Austral, University of Concepción, Concepción 4030000, Chile
9 Instituteof Oceanography and Climate Change, y Cambio Global, University of las Palmas de Gran Canaria, Las Palmas de Gran Canaria 35017, Spain
* Correspondence: camorale@udec.cl; Tel.: +5-641-266-1234

Received: 17 April 2018; Accepted: 22 May 2018; Published: 25 May 2018


**Abstract:** Understanding the influence of mesoscale and submesoscale features on the structure of phytoplankton is a key aspect in the assessment of their influence on marine biogeochemical cycling and cross-shore exchanges of plankton in Eastern Boundary Current Systems (EBCS). In this study, the spatio-temporal evolution of phytoplankton size classes (PSC) in surface waters associated with mesoscale eddies in the EBCS off central-southern Chile was analyzed. Chlorophyll-a (Chl-a) size-fractionated filtration (SFF) data from in situ samplings in coastal and coastal transition waters were used to tune a three-component (micro-, nano-, and pico-phytoplankton) model, which was then applied to total Chl-a satellite data (ESA OC-CCI product) in order to retrieve the Chl-a concentration of each PSC. A sea surface, height-based eddy-tracking algorithm was used to identify and track one cyclonic (sC) and three anticyclonic (ssAC1, ssAC2, sAC) mesoscale eddies between January 2014 and October 2015. Satellite estimates of PSC and in situ SFF Chl-a data were highly correlated ($0.64 < r < 0.87$), although uncertainty values for the microplankton fraction were moderate to high (50 to 100% depending on the metric used). The largest changes in size structure took place during the early life of eddies (~2 months), and no major differences in PSC between eddy center and periphery were found. The contribution of the microplankton fraction was ~50% (~30%) in sC and ssAC1 (ssAC2 and sAC) eddies when they were located close to the coast, while nanoplankton was dominant (~60–70%) and picoplankton almost constant (<20%) throughout the lifetime of eddies. These results suggest that the three-component model, which has been mostly applied in oceanic waters, is also applicable to highly productive coastal upwelling systems. Additionally, the PSC changes within mesoscale eddies obtained by this satellite approach are in agreement with results on phytoplankton size distribution in mesoscale and submesoscale features in this region, and are most likely triggered by variations in nutrient concentrations and/or ratios during the eddies' lifetimes.

**Keywords:** phytoplankton size classes; remote sensing; mesoscale eddies; coastal upwelling system; size-fractionated filtration data; Eastern Boundary Current Systems

## 1. Introduction

Physical dynamics in oceans promote processes of change and adaptation in biological systems at global and regional scales [1,2]. In the case of mesoscale structures (10–100 km, day-months), such as fronts and eddies, their movement through the ocean causes modifications in the physical properties (i.e., light, temperature) of the water column, changing nutrient conditions and, consequently, the phytoplankton community structure [3–5]. Mesoscale eddies occupy 25–30% of the surface ocean, contain more than 80% of the kinetic energy of oceanic circulation, and can generate different biological responses depending on eddy type (i.e., surface cyclonic/anticyclonic or subsurface anticyclonic eddy) [6–8]. Surface cyclonic (anticyclonic) eddies have been characterized by a negative (positive) sea level anomaly (SLA), a dome (bowl) shape of the isopycnals inducing upwelling (downwelling) at the eddy center, accompanied with an input (loss) of nutrients to the euphotic layer and a surface enhancement (diminishment) of chlorophyll-a (Chl-a) [9–12]. There is also a particular type of anticyclonic eddy, called intrathermocline (ITE) or subsurface mode water eddy, which represents 30–55% of the anticyclonic eddy population in Eastern Boundary Current Systems (EBCS) [13]. These eddies (ITEs) are characterized by a typical radius of ~20–60 km and have a vertical extent of ~500 m, together with dome-shaped isopleths in the upper layers and a bowl shape in the lower layers, a minimum in oxygen, and high rates of phytoplankton productivity [14–17].

Several mechanisms associated with mesoscale eddies have been proposed to modify primary production, carbon fluxes, and/or phytoplankton patterns (in terms of Chl-a). They include eddy trapping and stirring, which can lead to a dipole-like distribution of Chl-a at the eddy periphery associated with the trap and horizontal advection of waters with high or low Chl-a, caused by the rotation and direction of eddy propagation [11,18,19]. Other mechanisms involve a strong vertical exchange of waters, such as eddy pumping during eddy formation, generating a positive (negative) Chl-a monopole centered on the core of cyclonic (anticyclonic) eddies [10,20]. An opposite pattern is observed after the development phase, mainly in association with eddy-Ekman pumping due to the relative movement of the wind curl and eddy current velocity field [4,8,21–23]. Other important vertical exchanges of waters can be attributed to eddy-eddy interactions, which may also lead to frontogenesis, resulting in a convergent front between eddies and in an enhancement of Chl-a in the warm (anticyclonic) side and isopycnal subduction of Chl-a in the cold (cyclonic) side [24–27]. The impact that eddies have on the pelagic ecosystem has been mostly studied at the global scale and in open ocean environments [4,8] and, far less, in EBCS regions. Studies in EBCS have reported an exchange of chemical and biological properties between coastal and oceanic waters associated with the propagation of mesoscale eddies, e.g., [28–31]. Most of these studies are based on total Chl-a, and only a few have analyzed phytoplankton community structure within mesoscale eddies or other submesoscale features, e.g., [32–35]. The later, however, are restricted in space and time, mainly due to the difficulty in obtaining high-resolution, in situ data associated with the complete trajectory of eddies.

Over the last decade, a growing emphasis has been placed in the development of approaches to differentiate phytoplankton size classes (PSC) using satellite products, since phytoplankton size structure is an important indicator of the state of pelagic ecosystems and is strongly related to ocean carbon cycle, marine biogeochemistry, nutrient uptake, light absorption, primary production, and transfer of energy to higher trophic levels, e.g., [36–41]. These approaches have been based on (i) the optical signatures of phytoplankton groups using the spectral shape of phytoplankton absorption ($a_{ph}$: Phytoplankton Absorption spectra) to characterize the PSC, e.g., [36,42]; (ii) the relationship between Chl-a concentration by each PSC with total Chl-a (as an index of phytoplankton abundance

or biomass) using high performance liquid chromatography [HPLC] pigment and/or size-fractionated filtration (SFF) in situ data e.g., [43–45]; and (iii) the relationship between the phytoplankton groups and environmental factors (sea surface temperature or irradiance) e.g., [41,46]. Most of these approaches have been applied to open ocean waters, e.g., [41–45,47,48], while fewer ones have been including more information of coastal waters and have been mainly based on pigments or absorption spectra from in situ data [49–51]. Furthermore, only one recent study has used satellite estimates of PSC to infer shifts in the phytoplankton community related to a cyclonic eddy in oceanic waters [52].

In this study, for the first time, the three-component abundance-based model of Brewin et al. [43], developed for satellite ocean colour observations, was tuned for the highly productive coastal upwelling region off central-southern Chile, based on SFF in situ data, in order to estimate the Chl-a concentration of three phytoplankton size-groups [micro-, nano-, and pico-phytoplankton]. Additionally, we assess the changes in phytoplankton size structure throughout the lifetime of four different mesoscale eddies moving from the coastal zone (CZ; ~100 km from the coast) to the coastal transition zone (CTZ; coast to ~600 to 800 km offshore). We discuss the advantages/disadvantages of implementing an abundance-based model using SFF data in this EBCS, and we explore shifts in PSC associated with mesoscale features. We expect this study to contribute to improving regional biogeochemical models, since biological processes at the sub- and mesoscale levels are a key aspect of marine biogeochemistry, carbon export, and transfer of energy to higher trophic levels.

## 2. Data and Methodology

### *2.1. Study Area*

The selected study region off central-southern Chile (33–38°S, 72–80°W; Figure 1) is located in the Eastern South Pacific and includes several topographic features, in particular the following capes: Point Curaumilla (33°00′S), Point Topocalma (34°10′S), Point Nugurne (35°57′S), and Point Lavapié (37°15′S) [53]. The region between ~35–38°S is characterized by a strong seasonal coastal upwelling during the austral spring-summer months in response to the intensification of southwesterly winds [54,55]. Coastal upwelling and solar radiation promote the generation of an upwelling front in this region. Variations in the coastline orientation, bathymetry, general circulation, and mesoscale activity also influence front and eddy generation [56–58]. In the area off Point Lavapié, several cyclonic and surface/subsurface anticyclonic eddies are persistently generated in association with higher levels of eddy kinetic energy, and these features move seaward through the CTZ at a relatively low speed (~1.7 km $d^{-1}$) [15,30,32,59].

### *2.2. Satellite Model of Phytoplankton Size Classes*

#### 2.2.1. In Situ Chlorophyll-a Size-Fractionated Data

A total of 227 Chl-a size-fractionated data collected in the CZ and CTZ off central-southern Chile were used to tune and validate the three-component model of Brewin et al. [43]. Total and size-fractionated Chl-a in the micro- ($C_M$, >20 μm), nano- ($C_N$, 2 to 20 μm), and pico-phytoplankton ($C_P$, <2 μm) range were collected during different oceanographic campaigns in the region of study: (i) FIP Bio-Bio monitoring cruises (35.30–38°S, 72.38–78.29°W), between November 2004 and January 2009; (ii) PHYTOFRONT cruise (36.50–36.75°S, 73.10–74.51°W) from 3 to 7 of February 2014; (iii) FIP Seamounts cruise (33–34°S, 73.82–80°W), between 14 and 22 of September 2015; and (iv) COPAS (Centro de Investigación Oceanográfica Pacífico Sur-Oriental) time series at a fixed coastal station (St. 18; 36.50°S–73.13°W) from July 2004 to November 2009 (Figure 1).

The procedure for Chl-a SFF consisted in the following steps for analyses before 2015: (i) filtration (~250 mL) of water samples using GF/F glass fiber filters (<0.7 μm pore diameter) for total Chl-a; (ii) pre-filtration (~250 mL) through cellulose-ester filter (3 μm pore diameter) and then by GF/F glass fiber filters for the $C_p$; (iii) pre-filtration (~250 mL) through a NYTEX® type of mesh (20 μm pore

diameter) and then by GF/F glass fiber filters to obtain a combined $C_N$ and $C_P$ fraction. After this, the $C_N$ and $C_M$ fractions were obtained by subtracting $C_P$ from the combined $C_N$ and $C_P$ fraction and the latter from total Chl-a, respectively [60]. In 2015 (FIP Seamount cruise), sequential filtration systems were used, consisting of three different sizes of polycarbonate filters: 20 µm, 2 µm, and 0.2 µm allowing the derivation of $C_M$, $C_N$, and $C_P$ [61]. Pigment extraction was carried out in vials with a known volume of 90% acetone and maintained at −20 °C for 24 h, after which the samples were analyzed by fluorometry (Turner Design AU-10, Turner Design TD-700, or a Turner Design Trilogy). Fluorometer calibration was done before and after each cruise using a pure Chl-a standard. In all cases, duplicate or triplicate samples were taken at different depths within the upper 100 m depth; samples collected within the first 10 m of the upper layer were used in this study. Total in situ Chl-a concentration for the subsequent analyses was calculated as the sum of the Chl-a values contributed by each PSC [41,43,44].

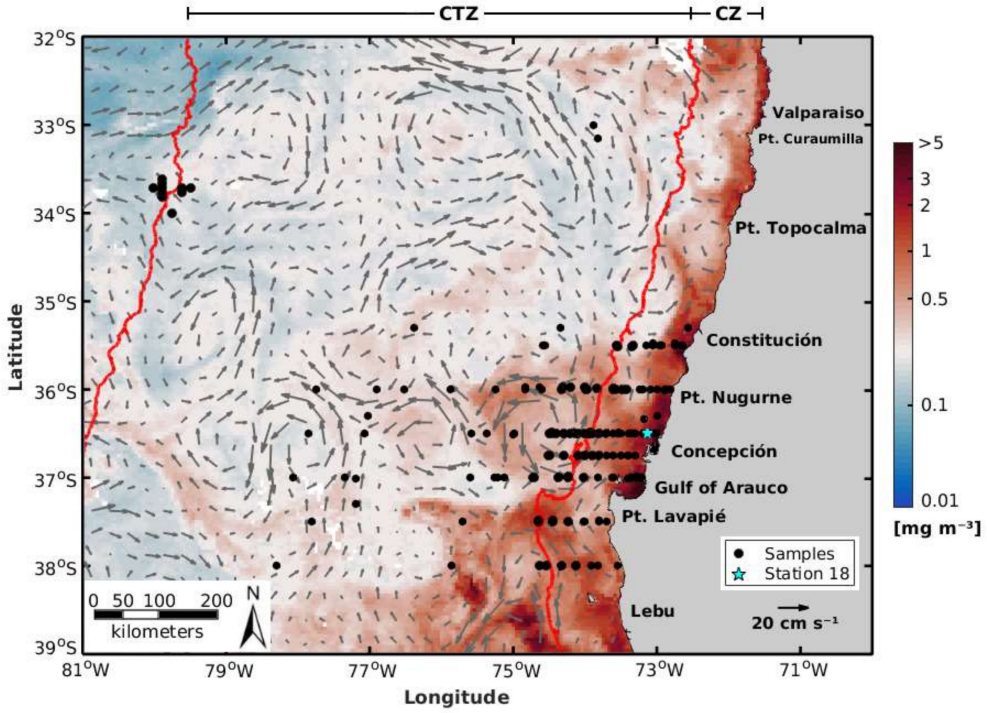


**Figure 1.** Study area in central-southern Chile. An eight-day composite (25 January 2014–1 February 2014) of surface total chlorophyll-a (Chl-a), obtained from version 3.0 of the Ocean Colour Climate Change Initiative (OC-CCI; 4 km resolution) product, is represented in red-blue color scale. The geostrophic velocity, obtained from Ssalto/Duacs multimission altimeter AVISO product (http://www.aviso.altimetry.fr), is shown in gray arrows. The blue star indicates the location of the COPAS coastal time series Station 18 and, together with the black dots, indicates the locations of the size-fractionated filtration (SFF) Chl-a in situ data ($\leq$ 10 m depth), during different campaigns (November 2004–September 2015). The red lines indicate the offshore limit of the coastal zone (CZ; ~100 km from the coast) and the coastal transition zone (CTZ; coast to ~800 km offshore), respectively.

### 2.2.2. Parameterization of the Three-Component Model

The two-component model of Sathyendranath et al. [62] was extended to a three-component model by Brewin et al. [43] to estimate the Chl-a concentration contributed by three PSC ($C_M$, $C_N$, and $C_P$) as a function of total Chl-a. The model is abundance-based and assumes that (i) the micro-(pico-) phytoplankton fraction increases (decreases) monotonically as a function of total Chl-a and (ii) smaller cells achieve a given Chl-a concentration, beyond which total Chl-a increases only by the addition of

larger size cells. The model is based on the following relationships: (i) total Chl-a concentration ($C$) is derived from the sum of the three PSC,

$$C = C_M + C_N + C_P \quad (1)$$

and (ii) two exponential functions are used to estimate the Chl-a concentration of the smaller PSC as a function of total Chl-a ($C$) [62]: one which combines the nano- and picoplankton groups ($C_{NP}$, [63]), and one for the picoplankton ($C_P$),

$$C_{NP} = C_{NP}^m \left[1 - exp\left(-\left(\frac{D_{NP}}{C_{NP}^m}\right)C\right)\right] \quad (2)$$

$$C_P = C_P^m \left[1 - exp\left(-\left(\frac{D_P}{C_P^m}\right)C\right)\right] \quad (3)$$

in which ${C_{NP}}^m$ and ${C_p}^m$ are the asymptotic maximum values for the associated size classes; $D_{NP}$ and $D_P$ reflect the fraction contributed by each size-class to total Chl-a as total Chl-a tends to zero, and they should take values in the range between 0 and 1 to ensure size-fractionated Chl-a does not increase faster than total Chl-a [41]. Equations (2) and (3) can also be expressed in terms of the fractions of each associated size class ($F_{NP}$ and $F_P$), i.e., the size-specific fractional (relative) contributions to total Chl-a, and can be calculated by dividing the size-specific Chl-a concentration ($C_{NP}$ and $C_p$) by $C$ [47,64]. Model parameters (${C_{NP}}^m$, ${C_P}^m$, $D_{NP}$, and $D_P$) were derived from Equations (2) and (3) in terms of the fractions fitted to $C$, $C_{NP}$, and $C_P$, using the in situ SFF Chl-a data. The fitting procedure used a standard, nonlinear least-squares method of Levenberg-Marquardt [43].

In order to compute the uncertainties in the parameters and to validate the model, the in situ SFF Chl-a data (227 samples) were randomly split, using 80% of the measurements (182 samples) for parameterization and the remaining 20% (45 samples) as the validation dataset (see Section 2.2.3). A bootstrapping method [65] was used to compute the model parameters and their uncertainties, so the 182 measurements were randomly sub-sampled with replacement (1000 times) and Equations (2) and (3) were re-fitted for each sub-sample by minimizing the squared difference in the fractions ($F$). Then, the median and 95% confidence intervals were calculated for the obtained parameter distribution [41].

#### 2.2.3. Validation of the Model, Application to Satellite Data, and Match-Up between In Situ and Satellite Size-Fractionated Chlorophyll-a Estimates

Total Chl-a from the parameterization dataset together with the model parameter values (${C_{NP}}^m$, ${C_p}^m$, $D_{NP}$, and $D_P$) were used as input variables in Equations (2) and (3) to calculate model estimates of $C_{NP}$ and $C_p$, after which $C_N$ and $C_M$ were derived from the following relationships $C_N = C_{NP} - C_P$ and $C_M = C - C_{NP}$ [41,43,48]. Modelled and in situ size-fractionated Chl-a data were compared to evaluate the PSC model performance [41,48]. The same procedure was carried out to calculate satellite size-fractionated Chl-a based on daily satellite-derived total Chl-a (January 2004 to December 2015) for the region of study. These data were obtained from version 3.0 of the Ocean Colour Climate Change Initiative (OC-CCI, a merged product available at http://www.oceancolour.org/), at processing level 3 and spatial resolution of 4 km. The in situ size-fractionated Chl-a validation dataset (45 samples) was compared with the obtained size-fractionated Chl-a satellite estimates [41,48]. Each in situ sample was matched with a daily satellite dataset using the nine pixels closest to the location of the sample, and only match-ups with a coefficient of variation <0.15 and 50% of valid data in the nine pixels were considered. The median Chl-a concentration of these pixels was taken as the satellite estimate and compared with in situ data [41,66]. Finally, the Pearson linear correlation coefficient (r), root mean square (RMS) error, and bias ($\delta$) were calculated in $\log_{10}$ space as statistical metrics for model and satellite model validation following Brewin et al. [48], in order to compare them with those from previous studies. Recently Seegers et al. [67] have queried the use of RMS as an error metric in the case of Chl-a data and have instead recommended the use of the mean/median absolute error (MAE

and MdAE) and the median bias (δ). In addition, these authors recommend that these metrics be back-transformed from the $\log_{10}$ space for interpretation. For this reason, we have also included the metrics and procedures suggested by Seegers et al. [67].

### 2.3. Eddy Detection and Tracking

Eddy detection and tracking was based on the freely-available sea surface height (SSH) approach of Mason et al. [68] (http://imedea.uib-csic.es/users/emason/py-eddy-tracker), which is based in the detection of closed contours of sea level anomaly (SLA), following the procedures described by Chelton et al. [19], Kurian et al. [69], and Penven et al. [70]. Daily delayed-time "two-sat" SLA data from the Ssalto/Duacs AVISO 2014 altimetry product (http://www.aviso.altimetry.fr), from January 2014 to December 2015, were used to represent the surface current in the study region, with the advantage that these data offer homogeneous quality in space and time, and enhance the description of mesoscale activity in coastal regions of EBCS [71].

Daily SLA fields were spatially high-pass filtered by removing a smooth field, obtained from a Gaussian filter with a zonal (meridional) major (minor) radius of 10° (5°) or ~1000 km (~500 km). SLA closed contours computed at 0.2 cm intervals and searched from 100 (−100) cm downward (upward) were used to identified cyclonic (anticyclonic) eddies. To be selected as the effective perimeter of an eddy, an identified closed contour should meet the following criteria: (i) the amplitude has to be >0.1 cm, (ii) the number of local extreme limited to 1, and (iii) the radius of the eddy has to range from 0.3° (~30 km) to 4.461° (~446 km) [68]. The lower value differs from that established by Chelton et al. [19], where eddies with radius <0.4° (~40 km) were filtered out. In this sense, the method of Mason et al. [68] has a natural tendency to identify more and smaller eddies than that of Chelton et al. [19], presumably due to stricter identification criteria and sharper SLA gradients in the version of the AVISO data (DT14) compared with the DT10 version used by Chelton et al. [19,71]. Moreover, we were interested in following specific eddies, including those subsurface-intensified but with limited surface signature, which justifies our choice of a minimum valid radius of 0.3° (~30 km). Also, in order to keep tracking an eddy even when punctually distorted, we chose not to use a shape test that aimed to filter out highly irregular closed contours [68], so the position of an eddy center and the speed-based eddy radius (the radius of the circle with the same area as the region within the contour of SLA with maximum rotational speed) were then followed along the eddy-track path of interest.

One cyclonic and three anticyclonic eddies were detected and tracked in the study region in the period between January 2014 and December 2015. Two of the anticyclones were found to be subsurface-intensified anticyclonic eddies, one of which interacted with an oceanic seamount at some point, as revealed by satellite and CTD (conductivity, temperature and depth) data collected during the FIP Seamount cruise [61], while the other interacted with an upwelling front, as observed in CTD data during the PHYTOFRONT cruise [33]. Specifically, the studied eddies are composed of (i) a subsurface anticyclone (ssAC1), which was born in the coastal region south of Point Lavapié (~38.04°S, 74.30°W) and propagated westward to the Juan Fernandez Ridge (27 December 2014 to 13 August 2015; 7.5 months of tracking); (ii) a subsurface anticyclone (ssAC2), which was initially detected off Point Nugurne (~36.21°S, 73.83°W; 1 January 2014 to 21 August 2014; 7.5 months of tracking); (iii) a surface anticyclone (sAC), which was born off Lebu (~38.67°S, 74.45°W; 10 February 2014 to 1 November 2014; 8.5 months of tracking); and iv) a surface cyclone (sC) detected close to Constitución (~35.14°S, 72.83°W; 9 November 2014 to 8 October 2015; ~11 months of tracking; Figure 1).

### 2.4. Size-Fractionated Chlorophyll-a Satellite Estimates in Mesoscale Eddies

Based on the spatial dimension of the study region (5° latitude × 8° longitude; 33–38°S, 72–80°W) and in order to remove unwanted small and large-scale features unrelated with mesoscale variability [8,19,22], the following procedure was carried out: (i) the seasonal cycle of the satellite estimates of size-fractionated Chl-a concentrations ($C_M$, $C_N$, and $C_P$) was removed by substracting

the monthly climatology (linearly interpolated to daily values) from the daily size-fractionated Chl-a data and (ii) eight-day composites of the satellite estimates resulting from the previous step were produced (for further details see Appendix A). For this purpose, the monthly climatology and the averages were calculated in $\log_{10}$ space, considering that Chl-a concentration is approximately log-normally distributed over the global ocean [72]. Also, an eight-day average of the radius (km) and the displacement speed (km week$^{-1}$) of eddies were calculated in order to have the same temporal resolution as the Chl-a data.

The obtained mesoscale size-fractionated Chl-a fields, sampled on a square grid (longitude × latitude), were placed in a framework of polar coordinates with a radial distance from the eddy center defined by the eddy radius (R), so the associated size-fractionated Chl-a fields were projected into an eddy frame and the Chl-a values at any distance r were projected to r/R. However, to be able to construct a standard scale based on the eddy radius of each eddy, we normalized the Chl-a fields by twice the radius (2R) in each case [8,22,73]. Then, we ensured that during the tracking period of eddies, the size-fractionated Chl-a fields covered at least 50% of their spatial extension, screening out the periods (weeks) when this was not achieved. Finally, the variability of PSC was evaluated from the average fraction fields ($F_M$, $F_N$, and $F_P$) in the eddy center ($r/R \leq 1$) and in the periphery ($1 < r/R \leq 2$), and these values were compared with the mean of the fractions in the CZ when eddies were located closer to the coast.

A flow-diagram of the methods described above and a list of symbols and abbreviations are presented in Appendixs B and C, respectively.

## 3. Results

In situ data of total and size-fractionated Chl-a concentrations analyzed in this study were mainly obtained in the CZ (77%), with total Chl-a values ranging between 0.20 and 17.76 mg m$^{-3}$, while the remaining (23%) correspond to the CTZ, with values between 0.15 and 1.66 mg m$^{-3}$ (Figure 1). The ~90% of the data were obtained during the spring-summer months, when the southwesterly winds favor the coastal upwelling. For this dataset, the contribution of each PSC in the study region was 35.4% by the microplankton fraction, with a mean (maximum) Chl-a concentration of 1.62 mg m$^{-3}$ (16.42 mg m$^{-3}$); 53.7% by nanoplankton, with a mean (maximum) Chl-a concentration of 0.84 mg m$^{-3}$ (4.42 mg m$^{-3}$); and 10.9% by picoplankton, with mean (maximum) Chl-a values of 0.12 mg m$^{-3}$ (0.87 mg m$^{-3}$).

### 3.1. Satellite Model of Phytoplankton Size Classes

In situ Chl-a concentration by size ($C_M$, $C_{NP}$, $C_N$, and $C_P$), and by fractions ($F_M$, $F_{NP}$, $F_N$, and $F_P$), as a function of in situ total Chl-a, together with the re-tuned three-component model of Brewin et al. [43], are shown in Figure 2. The general trends of these relationships were captured by the model based on the calculated regional parameters (Table 1), according to which the nano- and picoplankton reached asymptotic values of ${C_{NP}}^m$ ~2.12 mg m$^{-3}$ and ${C_P}^m$ ~0.19 mg m$^{-3}$, while Chl-a concentrations higher than these were only achieved by the micro-phytoplankton (Figure 2a–d). In terms of fractions, the model also captured the trends of the in situ dataset, with large (small) cells increasing (decreasing) their contribution to total Chl-a as its values became higher (Figure 2e–h). The parameter $D$ also reflects the higher contribution by the smaller fractions when total Chl-a tends to zero ($D_{NP}$ ~0.92 and $D_P$ ~0.21; Table 1 and Figure 2f,h).

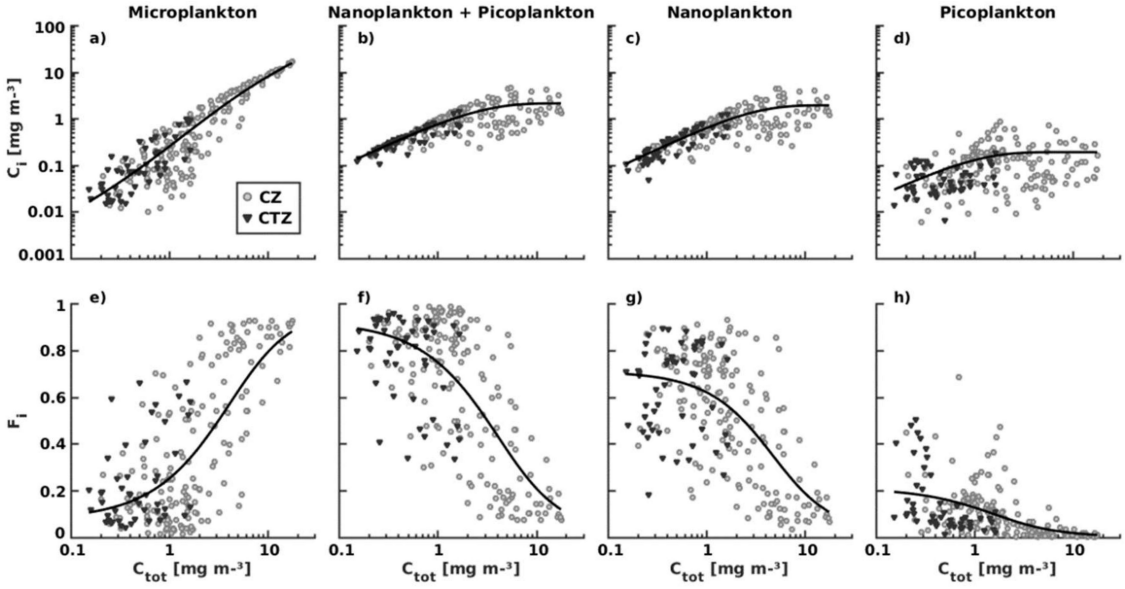


**Figure 2.** In situ concentrations of size-fractionated Chl-a for micro- ($C_M$), nano- and pico- ($C_{NP}$), nano- ($C_N$), and picoplankton ($C_P$) (upper panels: **a**–**d**), and their contribution to total in situ Chl-a (lower panels: **e**–**h**) as a function of total in situ Chl-a concentration ($C$). The fitted three-component model of Brewin et al. [43] is overlaid in each case (solid black line). The subscript 'i' indicates the different Chl-a size classes. The location of the samples in the CZ and CTZ is differentiated by grey dots and black triangles, respectively.

**Table 1.** Parameter values for the three-component model based on in situ size-fractionated chlorophyll-a (Chl-a) concentrations off central-southern Chile and comparison with those derived from previous studies in different systems.

| | | | Model Parameters | | | |
|---|---|---|---|---|---|---|
| | **Area** | **Method** | $C_{NP}^m$ **(mg m$^{-3}$)** | $D_{NP}$ | $C_P^m$ **(mg m$^{-3}$)** | $D_P$ |
| Brotas et al. [50] $ | EA | HPLC | 0.36 | 0.92 | 0.07 | 0.77 |
| Lin et al. [52] | SCS | HPLC | 0.95 | 0.94 | 0.26 | 0.90 |
| Brewin et al. [44] | AO | SFF | 2.78 (2.23–3.56) | — | 0.66 (0.55–0.80) | — |
| Brewin et al. [41] | Global | HPLC | 0.77 (0.72–0.84) | 0.94 (0.93–0.95) | 0.13 (0.12–0.14) | 0.80 (0.78–0.82) |
| Brito et al. [51] $ | NEA | $a_{ph}$, HPLC | 0.26–0.50 | 0.86 | 0.09 | 0.16 |
| Ward [46] | Global | SFF | 0.79 | 0.97 | 0.16 | 0.84 |
| Brewin et al. [48] | NA | HPLC, SFF | 0.82 (0.76–0.88) | 0.87 (0.86–0.89) | 0.13 (0.12–0.13) | 0.73 (0.71–0.76) |
| This study | CSC | SFF | 2.12 (1.75–2.54) | 0.92 (0.88–0.96) | 0.19 (0.11–0.27) | 0.21 (0.16–0.33) |

$C^m$ indicates the asymptotic maximum of Chl-a for a given size class ($P$ = pico-phytoplankton; $NP$ = nano- + pico-phytoplankton), and $D$ reflects the fraction contributed by a given size class to total Chl-a as total Chl-a tends to zero. In brackets are the 95% confidence intervals calculated for the obtained parameters distribution. In situ methods to derive size-specific Chl-a concentrations: HPLC = High Performance Liquid Chromatography, SFF = Size-Fractionated Filtration, and $a_{ph}$ = Phytoplankton Absorption spectra. Study areas: EA = Eastern Atlantic, SCS = South China Sea, AO = Atlantic Ocean, NEA = North-East Atlantic, NA = North Atlantic, and CSC = Central-Southern Chile. $ Studies that include coastal stations for in situ size-specific Chl-a measurements.

The PSC model validation with regard to in situ size-fractionated Chl-a concentrations was assessed with statistical metrics (r, RMS error, MdAE, and MAE) without back-transformation from $\log_{10}$ space, and the results are presented in Table 2 and compared with previous studies. Higher correlation coefficients (r) were obtained for the micro-, nano-, and the combined nano- and picoplankton groups (>0.80), while that of picoplankton was (<0.4). Low uncertainties values were obtained for the nano- and the combined nano- and picoplankton groups, whereas those of the micro- and picoplankton were moderate. Biases (δ) were mostly low for the different PSC (0.04 for nano- and pico, 0.17 for pico-, 0.05 for nano-, and 0.13 for microplankton). Our correlation and uncertainty values are similar to those reported in previous studies (Table 2), except for the low r value in the case of

the picoplankton. The latter value is, however, higher than that obtained by Ward [46]. In applying the back-transformation procedure recommended by Seegers et al. [67], we considered the metrics MdAE and bias for comparison (Table 3). In the interpretation of these metrics (MdAE(t) and δ(t)), values closer to unity indicate lower relative errors and bias, with biases higher (lower) than unity implying that the model overestimates (underestimates) in situ measurements [67]. In terms of the MdAE(t) results, the highest uncertainties were associated with the micro- (~69%) and picoplankton (~97%) size classes in comparison with the other PSC (<30%); bias values were close to unity, except for picoplankton (Table 3).

**Table 2.** Statistical relations between modelled and in situ size-fractionated Chl-a concentrations and comparison with those obtained in previous studies.

| | | Metrics | | |
|---|---|---|---|---|
| | | **r** | **RMS** | **MAE** |
| Micro | Brotas et al. [50] $ | — | — | 0.32 |
| | Lin et al. [52] | 0.99 | 0.46 | — |
| | Brewin et al. [41] | 0.91 | 0.34 | — |
| | Ward [46] | 0.83 | 0.47 | — |
| | Brewin et al. [48] | 0.93 | 0.32 | — |
| | This study | 0.88 | 0.41 | 0.30 (0.23) |
| Nano | Brotas et al. [50] $ | — | — | 0.19 |
| | Lin et al. [52] | 0.94 | 0.17 | — |
| | Brewin et al. [41] | 0.93 | 0.24 | — |
| | Ward [46] | 0.78 | 0.30 | — |
| | Brewin et al. [48] | 0.88 | 0.30 | — |
| | This study | 0.80 | 0.22 | 0.16 (0.11) |
| Pico | Brotas et al. [50] $ | — | — | 0.18 |
| | Lin et al. [52] | 0.89 | 0.39 | 0.04 |
| | Brewin et al. [41] | 0.64 | 0.26 | — |
| | Ward [46] | 0.21 | 0.43 | — |
| | Brewin et al. [48] | 0.56 | 0.34 | — |
| | This study | 0.37 | 0.42 | 0.33 (0.29) |
| Nano + Pico | Brotas et al. [50] $ | — | — | 0.11 |
| | Lin et al. [52] | — | — | 0.03 |
| | Brewin et al. [41] | 0.94 | 0.13 | — |
| | Ward [46] | 0.88 | 0.12 | — |
| | Brewin et al. [48] | 0.90 | 0.19 | — |
| | This study | 0.81 | 0.20 | 0.14 (0.10) |

r = Pearson linear correlation coefficient, RMS = root mean square error, MAE = mean absolute error, and MdAE = median absolute error in brackets. Statistical test in $\log_{10}$ space. $ Studies that include coastal stations for in situ size-specific Chl-a measurements.

**Table 3.** Statistical relations between modelled and in situ size-fractionated Chl-a concentrations back-transformed from $\log_{10}$ space.

| | Metrics | |
|---|---|---|
| | **MdAE (t)** | **δ (t)** |
| Micro | 1.69 | 1.07 |
| Nano | 1.30 | 0.98 |
| Pico | 1.97 | 1.36 |
| Nano + Pico | 1.27 | 0.97 |

MdAE(t) = median absolute error and δ(t) = median bias, both back-transformed from $\log_{10}$ space (t).

Satellite total Chl-a and model PSC estimates against in situ Chl-a concentrations are displayed in Figure 3. Together with this, the PSC satellite model validation with regard to in situ Chl-a concentrations was assessed with statistical metrics (r and RMS error without back-transformation from $\log_{10}$ space; MdAE and bias with and without back-transformation), and the results are presented in Table 4 and compared with previous studies. Satellite and in situ total Chl-a displayed the highest correlation and lowest uncertainties. Similar values were obtained for nano- and picoplankton groups ($r > 0.70$; RMS < 0.30; MdAE < 0.18; Figure 3c–e). In the case of the metrics without back-transformation, the microplankton value for r was relatively high, but the uncertainty values were moderate compared to the smaller PSC. The latter is in coherence with a higher data dispersion for this fraction when Chl-a values are <0.1 mg $m^{-3}$ (Figure 3b). Biases (δ) were close to zero for total Chl-a and PSC. In addition, the PSC satellite model validation was performed considering meridional (Northern, Center, and Southern areas of the study region), zonal (CZ and CTZ), and seasonal (calendar seasons) differences. However, no changes were detected in data dispersion (not shown). In comparison with the statistical metrics from previous studies, similar values for r and uncertainty were observed for total Chl-a and PSC; Brotas et al. [50] have reported a similar uncertainty value for the microplankton (48%) compared to ours. In the case of the statistical back-transformed metrics (MdAE(t) and δ(t)), moderate uncertainties (~50%) were observed for total Chl-a and the smaller PSC, whereas those of the microplankton were higher (>100%). The bias values were mostly low (<30%).

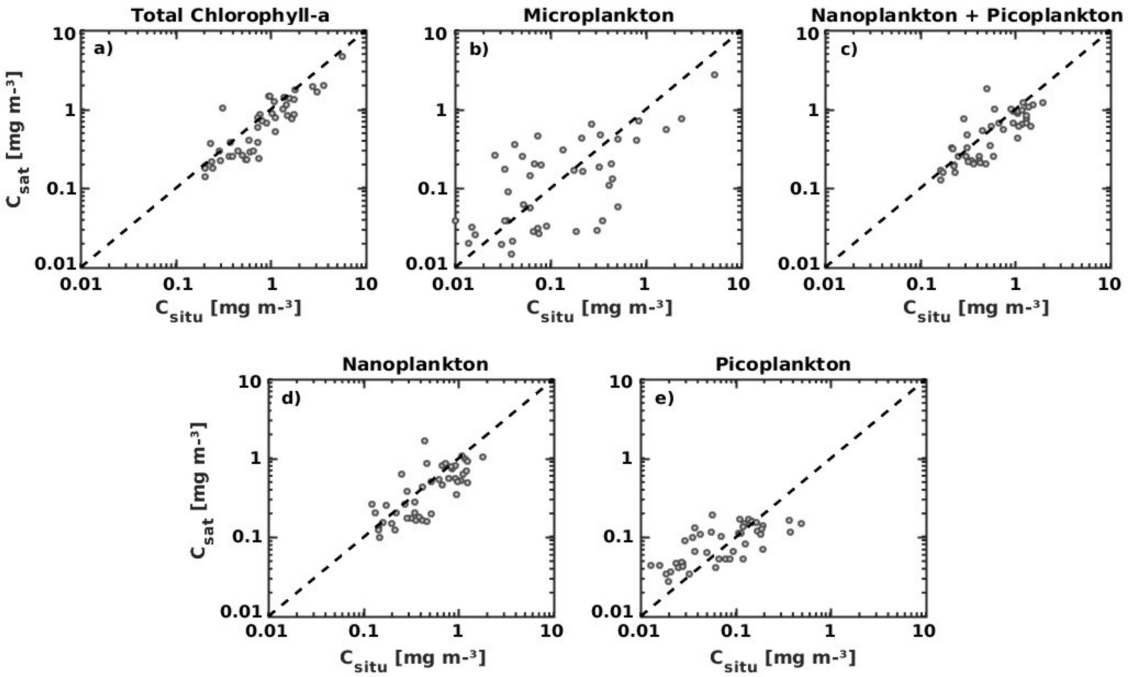


**Figure 3.** Total satellite Chl-a concentration (OC-CCI product; 4 km resolution) and size-fractionated Chl-a estimates obtained from the regional three-component model, as a function of in situ total and size fractioned Chl-a concentration. The black dotted line represents the 1:1 line (perfect relationship between in situ and satellite estimates).

**Table 4.** Statistical relations between the satellite estimates of phytoplankton size classes (PSC) from the regional re-tuned three-component model and in situ size-fractionated Chl-a concentrations and comparison with those obtained in previous studies.

| | Brewin et al. [41] | | Brewin et al. [48] | | This Study | | | | | |
|---|---|---|---|---|---|---|---|---|---|---|
| | r | RMS | r | RMS | r | RMS | MdAE | δ | MdAE (t) | δ (t) |
| Total | 0.88 | 0.25 | 0.86 | 0.29 | 0.87 | 0.22 | 0.15 | −0.12 | 1.42 | 0.73 |
| Micro | 0.86 | 0.41 | 0.85 | 0.45 | 0.64 | 0.50 | 0.36 | −0.01 | 2.34 | 0.92 |
| Nano | 0.80 | 0.38 | 0.76 | 0.43 | 0.79 | 0.22 | 0.17 | −0.09 | 1.49 | 0.79 |
| Pico | 0.57 | 0.28 | 0.49 | 0.35 | 0.72 | 0.28 | 0.18 | 0.06 | 1.54 | 1.14 |
| Nano + Pico | 0.79 | 0.27 | 0.76 | 0.30 | 0.76 | 0.24 | 0.16 | −0.08 | 1.45 | 0.77 |

r = Pearson linear correlation coefficient, RMS = root mean square error. Median absolute error and bias without back-transform from $\log_{10}$ space (MdAE and δ) and back-transformed (MdAE(t) and δ(t)).

An example of the spatial distribution of the satellite estimates for each PSC in the study region is presented in Figure 4. The highest Chl-a concentrations (5.56 mg $m^{-3}$) are contributed by the microplankton fraction in accordance with the model, and they are mostly observed in the CZ (Figure 4a,d). In contrast, intermediate and lower Chl-a values (< 5 mg $m^{-3}$) are mainly achieved by the nano- and picoplankton groups, which are widely distributed in the study region, but with a clear spatial dominance of the nanoplankton (Figure 4b,c,e,f).

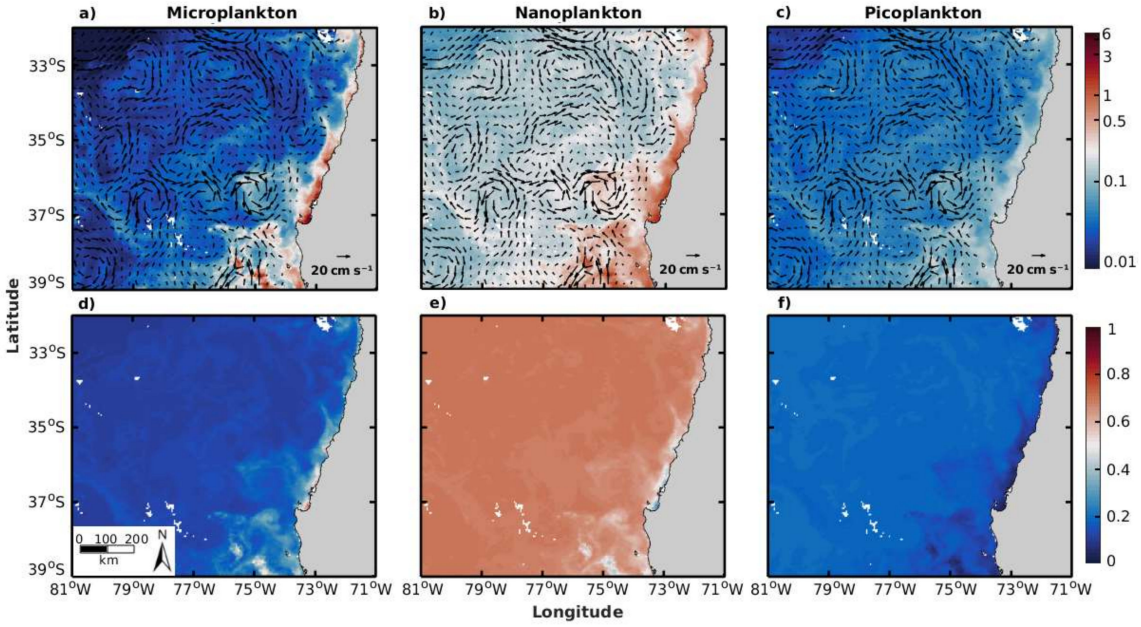


**Figure 4.** Spatial distribution of the satellite Chl-a estimates for size-fractionated concentrations (**a**–**c**; mg $m^{-3}$) obtained from the regional three-component model applied to the total Chl-a satellite data, and their relative contribution to total Chl-a (**d**–**f**; dimensionless). The geostrophic velocity field is shown (black arrows). Data in this figure are an example of an eight-day composite for the same dates included in Figure 1.

### *3.2. Spatio-Temporal Evolution of Phytoplankton Size Classes within Mesoscale Eddies*

The main features and trajectory of the studied eddies, such as the radius and the seaward velocity of displacement, are shown in Figure 5. These eddies move offshore at mean speeds of ~20 km $week^{-1}$ (~2.5 km $d^{-1}$) and have mean radius of ~40–60 km (~80–120 km in diameter). For the study period, the trajectories of the four eddies were independent of each other, except for ssAC2 and sAC, which were found to interact with each other during 25 weeks (~6 months; 10 February 2014

to 28 August 2014; data not shown). Also, the sAC eddy was detected and tracked farthest from the coast (~75°W) in comparison with the other eddies (upper panels in Figure 5).

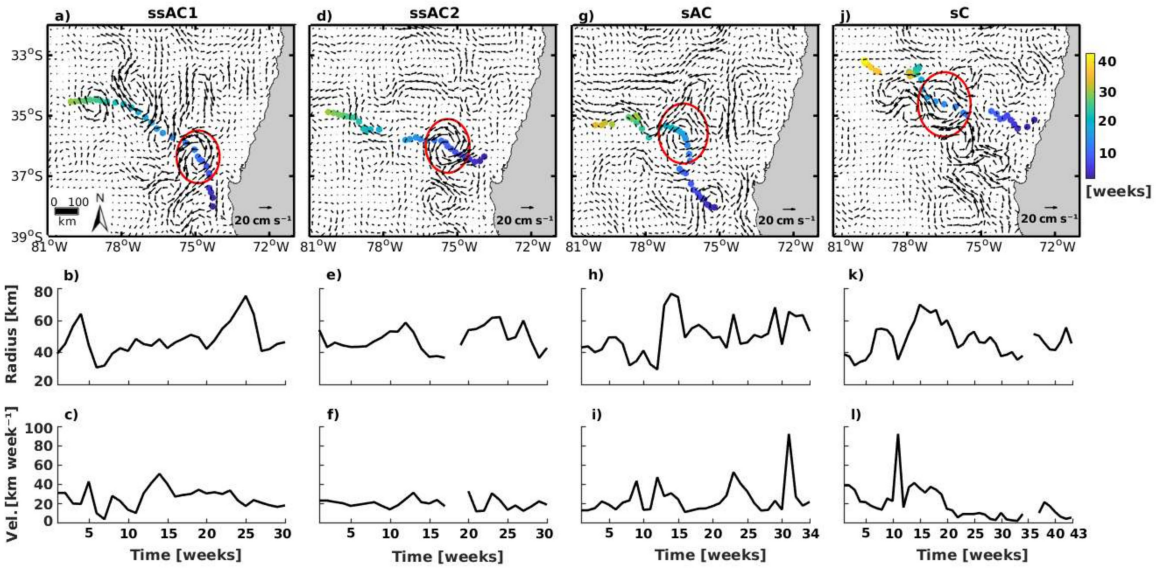


**Figure 5.** The geostrophic velocity field (black arrows) and the trajectories of the tracked mesoscale eddies (upper panels: **a**,**d**,**g**,**j**), together with radius (**b**,**e**,**h**,**k**) and displacement velocity (**c**,**f**,**i**,**l**) through time (in weeks). The red circles in the upper panels represent the eddies in a time step of their complete trajectories (blue-yellow color scale). Four eddies were analyzed: subsurface anticyclone 1 (ssAC1; 27 December 2014 to 13 August 2015, 30 weeks), subsurface anticyclone 2 (ssAC2; 1 January 2014 to 21 August 2014, 30 weeks), surface anticyclone (sAC; 10 February 2014 to 1 November 2014, 34 weeks), and surface cyclone (sC; 9 November 2014 to 8 October 2015, 43 weeks). Gaps in the data for some periods (weeks) were created after screening out size-fractionated Chl-a fields that did not cover at least 50% of the spatial extent of an eddy.

Eight-day composites of surface total Chl-a anomalies for three different time steps of the eddy trajectories, together with the mean surface currents, are shown in Figure 6, in order to visualize and compare total Chl-a anomalies within the eddies and those in the surrounding waters. High positive Chl-a anomalies (>1 mg $m^{-3}$) were mainly observed in ssAC1 and sC when they were located closer to the coast (Figure 6a,j), while lower values were found in ssAC2 and sAC for the first evaluated time step in comparison with those in the surrounding waters (Figure 6d,g). For the other time steps (middle and bottom panels in Figure 6), positive values were observed within and outside the eddies, except for the second evaluated time step in ssAC1, which showed negative anomalies (~−0.2 mg $m^{-3}$; Figure 6b) and for sC, where positive anomalies values were found (~0.6 mg $m^{-3}$; Figure 6k).

The evolution of each phytoplankton size fraction (as fractions of total Chl-a) within the eddies (center and periphery) is shown in Figure 7, along with the mean contribution by each fraction in the CZ for the first week of the eddy tracking period (red dots). No major differences in PSC were found between the center and the periphery of the eddies. The picoplankton fraction was in almost constant proportion (~0.10–0.20) with respect to the other groups, and a clear dominance of the nanoplankton was found in all the eddies (~0.50 to 0.70). For ssAC1 and sC eddies, the highest values by the microplankton fraction were of ~0.50 within the first 5 to 10 weeks of tracking (Figure 7a,j), in association with their closer proximity to the CZ (Figure 5a,j), while the nanoplankton display values of ~0.50 and the picoplankton fraction reached values <0.1 (Figure 7b,c,k,l). Inside these eddies, 20% more of the microplankton fraction is observed when compared with the CZ values (~0.33 and 0.26, respectively). For the subsurface anticyclone ssAC2, the microplankton (nano- and picoplankton) fraction showed a tendency to decrease (increase) along the tracking period (30 weeks;

Figure 7d,f), while for the surface anticyclone sAC, a decrease (increase) of the microplankton (nano- and picoplankton) fraction was detected during the first 10 weeks (Figure 7g–i).

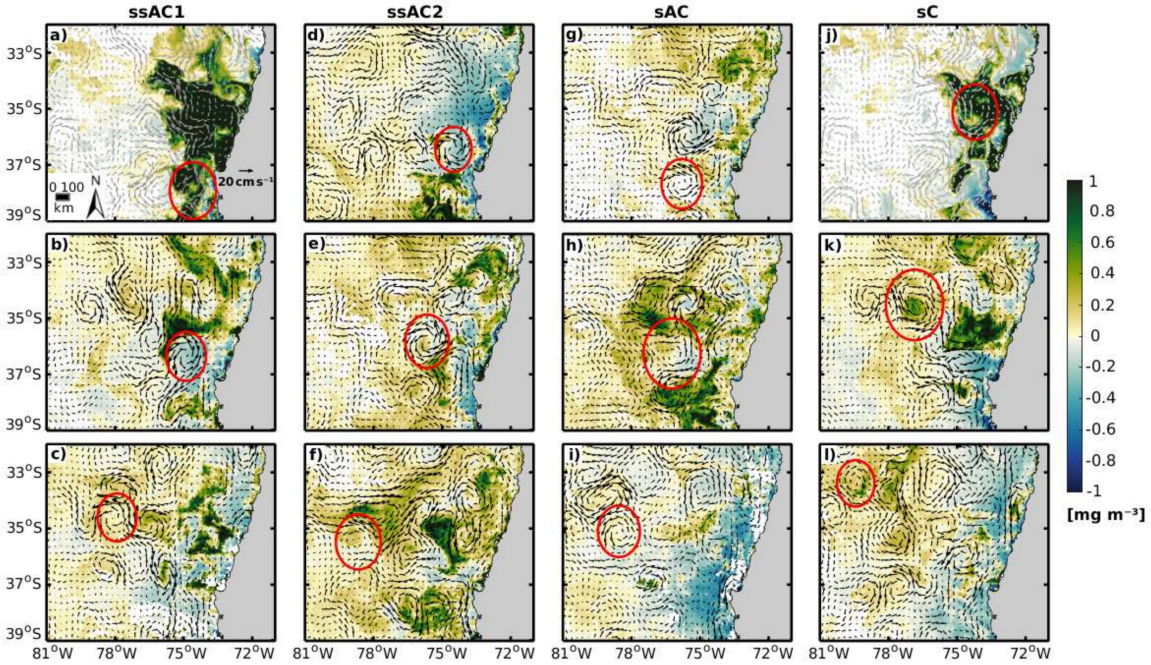


**Figure 6.** Eight-day composites of surface total Chl-a anomalies (green-blue color scale) for three different time steps of eddies trajectories. The position and radius of the eddies in each composite (red circles) and the geostrophic velocity field (gray/black arrows) are also shown. The dates of the composites are ssAC1 (**a**–**c**) 9–16 January 2015, 14–21 March 2015 and 2–9 June 2015; ssAC2 (**d**–**f**) 25 January to 1 February 2014, 22–29 March 2014 and 10–17 June 2014; sAC (**g**–**i**) 14–21 March 2014, 17–24 May 2014 and 29 August to 5 September 2014; and sC (**j**–**l**) 1–8 January 2015, 26 February to 5 March 2015 and 29 August to 5 September 2015.

After the first week of eddy-tracking, a decrease (increase) of the microplankton (nano- and picoplankton) fraction in the surface and subsurface anticyclones (ssAC1, ssAC2, and sAC) was found. A decrease (~15%) in the contribution of larger cells was found at the end of the tracking period for ssAC2 and sAC when compared with their initial CZ values (0.28–0.30; Figure 7d,g), and a larger reduction (~40%) when compared with the highest contribution achieved by the microplankton fraction (~0.50) in ssAC1 (Figure 7a). In terms of smaller fractions, an increase (~10%) was found between the initial CZ values and their final contribution (Figure 7b,c,e,f,h,i). Moreover, in the sC a decrease (increase) of the microplankton (nano- and picoplankton) fraction was also observed after the first ~10 weeks of tracking, but then the fractions were almost constant through the remaining period (Figure 7j–l). Specifically, a ~10% reduction in the microplankton contribution was found at the end of the 43 weeks when compared with the CZ value (0.26), and a ~40% decrease when compared with the highest contribution achieved by the microplankton inside the sC eddy (~0.50; Figure 7j). As well as in the anticyclones, the smaller fractions in the sC showed an increase (~10%) in comparison with the CZ values (~0.60 for nano- and ~0.10 for picoplankton; Figure 7k,l).

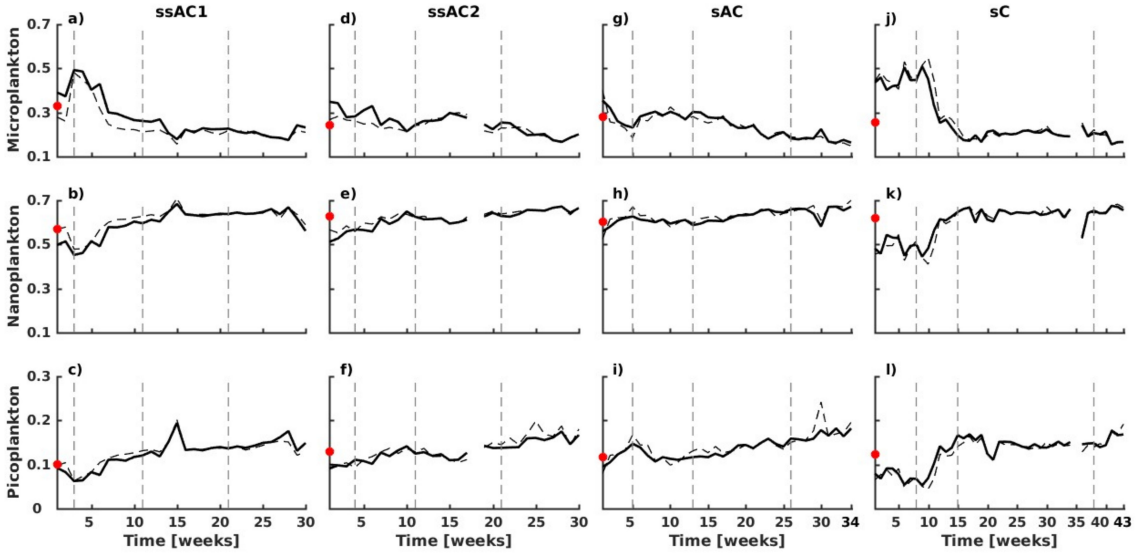


**Figure 7.** Temporal variability of phytoplankton size classes (PSC) in terms of the size-specific fractional (relative) contributions to total Chl-a (dimensionless) in the four selected eddies (center: continuous black line; periphery: dashed black line) during the period indicated in Figure 5. The mean contribution by each fraction in the CZ for the first week of eddy tracking is denoted by the red dots. The vertical dashed gray lines indicate the weeks of the composites of surface total Chl-a anomalies presented in Figure 6. Gaps in the data are explained in Figure 5.

## 4. Discussion

### *4.1. Application of a Three-Component Abundance-Based Model to Retrieve Satellite Estimates of Phytoplankton Size Classes in the Region off Central-Southern Chile*

Most of the previous studies using the three-component model have been based on Chl-a data from oceanic waters, e.g., [41,43,44,48,52] and very few have included data from coastal waters [50,51]. Total Chl-a values in this study (0.1 to 18 mg $m^{-3}$) include coastal and coastal transition waters in the Humboldt EBCS [74]. Our in situ dataset supports the model assumptions, i.e., that size-fractionated Chl-a co-varies with total Chl-a and that smaller cells achieve a given Chl-a concentration beyond, which total Chl-a increases only by the addition of larger size cells [43]. Differences between the model parameters obtained in our study with those from previous ones are mainly explained by regional characteristics (i.e., coastal vs oceanic) and/or the technique used to obtain size-fractionated Chl-a concentrations.

The asymptotic maximum of Chl-a for the two smaller PSC in this study ($C_{NP}{}^{m}$ ~2.12 mg $m^{-3}$) is similar to that found in the Atlantic Ocean by Brewin et al. [44] ($C_{NP}{}^{m}$ ~2.78 mg $m^{-3}$), both using the in situ SFF method to derive size-specific Chl-a concentrations (Table 1). In contrast, Ward [46] found a lower asymptotic value ($C_{NP}{}^{m}$: 0.79 mg $m^{-3}$) using the same technique, but the measurements excluded eutrophic and coastal areas. In comparison with studies using HPLC, $a_{ph}$, or a combination of both techniques, our $C_{NP}{}^{m}$ value was almost twice as large as results from oceanic regions ($C_{NP}{}^{m}$ ~0.77–0.95 mg $m^{-3}$) [41,48,52] and even larger than those from near-shore or upwelled coastal waters in the North-East/Eastern Atlantic ($C_{NP}{}^{m}$ ~0.26–0.50 mg $m^{-3}$) [50,51]. Our estimate of the asymptotic maximum of Chl-a for the picoplankton ($C_{P}{}^{m}$ ~0.19 mg $m^{-3}$) is in the range of those in previous studies ($C_{p}{}^{m}$ ~0.07–0.26 mg $m^{-3}$) [41,46,48,50–52], except for that of Brewin et al. [44] ($C_{P}{}^{m}$ ~0.66 mg $m^{-3}$). However, Brewin et al. [44] found higher asymptotic values for SFF data compared with HPLC data in both smaller size fractions ($C_{NP}{}^{m}$: ~2.78 mg $m^{-3}$ with SFF and ~1.41 mg $m^{-3}$ with HPLC, $C_{P}{}^{m}$: ~0.66 mg $m^{-3}$ with SFF and ~0.16 mg $m^{-3}$ with HPLC). Altogether, different techniques generate changes in the computed parameters of the three-component model.

The size-fractionated filtration (SFF) technique directly provides the size classes of phytoplankton, but it has uncertainties associated with inaccurate pore sizes of filters, cell breakage during filtration, and filter clogging, all errors that are very difficult to quantify [41,44,45,48]. In the case of the HPLC technique, size-fractionated Chl-a is inferred indirectly from specific pigments. However, most of these pigments are distributed in different phytoplankton size classes; therefore, a bias can be created [41,43,50]. The biases associated with these two methodological approaches overestimates or underestimates size-specific Chl-a concentrations, e.g., [44,45]. An alternative method, the $a_{ph,}$ has the advantage of being independent of total Chl-a concentration for distinguishing the PSC. However, absorption coefficients that are considered specific to a given PSC may include other size classes as a result of the package effect, which can modify the absorption spectrum, thereby generating uncertainties in the discretization of PSC [75,76]. Future work should focus on intercomparisons of the estimates of PSC in the region of study using different in situ methods and quantifying the uncertainties associated with them, as to improve the accuracy of model parameters [45,77].

In terms of the fractional contribution of the two smaller PSC to total Chl-a when total Chl-a tends to zero, the $D_{NP}$ parameter value obtained in this study (~0.92) is very similar to those from previous studies (~0.86–0.97) [41,44,46,48,50–52], without differences among techniques or regions (Table 1). In contrast, the $D_P$ parameter revealed regional differences. High $D_P$ values (~0.80–0.90) have been obtained in open ocean waters, e.g., [41,46,52], in consistency with the expected dominance of the picoplankton fraction in these environments [78–80]. However, Brotas et al. [50] also obtained a high $D_P$ value (0.77) in waters of a wide range of trophic status (from eutrophic to oligotrophic). Microscopic and flow cytometry analysis by these authors indicated that the picoplankton contributed to 90% of total cell abundance, but with a low contribution to total Chl-a ($C_p{}^m$ ~0.07 mg $m^{-3}$). Our estimate of $D_P$ (~0.21) is low and similar to that obtained in the coastal region off Portugal ($D_p$ of 0.16) [51]. Low $D_P$ values imply a higher contribution by the nanoplankton fraction, i.e., high ($D_{NP}$-$D_P$) values. In our study region, the nano- and microplankton fractions have been found to be dominant during the upwelling season [81–84].

The modelled size estimates obtained from the application of the three-component model tuned to the region off central-southern Chile show moderate uncertainty values with in situ Chl-a concentrations for the micro- and picoplankton fractions compared with the other groups (Tables 2 and 3). This could be partially explained by a higher dispersion of the in situ measurements in both PSC. In the case of picoplankton, this problem is detected in the whole range of total Chl-a, making it difficult to adjust an accurate monotonic function for this fraction. This also implies an error in the microplankton model estimates, since they are obtained by subtracting the picoplankton model estimates from in situ total Chl-a measurements. The same problem in the adjustment of a monotonic function for the picoplankton was reported by Ward [46], who used the SFF technique (as in this study) to distinguish in situ PSC. This gives support to the issue that the different in situ methods used to retrieve PSC could imply further uncertainties ([41,44,45,48], this study). Additionally, Ward [46] found a better performance of the three-component model when temperature ranges were incorporated, but reported that this factor is not important for tropical and sub-tropical regions, such as our study region. Altogether, improvements are required in the application of the PSC models, including a wider range of in situ total Chl-a concentrations or direct biomass estimates per size fractions in the region.

Regarding the satellite size model estimates, the moderate to high uncertainty values for the microplankton could be related to a wider dispersion of the satellite estimates for this fraction when total Chl-a reaches values <1 mg $m^{-3}$. In coastal upwelling regions, such as in this study, total Chl-a values reach up to 50 mg $m^{-3}$ [85], implying that the range included here is very narrow. The accuracy in the estimates for all PSC could be also related to (i) deviations in the relationship between the PSC and total Chl-a previously reported for optically complex waters, often found in coastal systems [48]; (ii) the spatial scale when comparing 4 km satellite pixels with specific in situ value obtained from ~250–300 mL of water, involving an additional sub-pixel variability in PSC estimates [48]; (iii) the estimation of total Chl-a concentrations from the ocean colour algorithms which

are based on an assumed relationship between the total Chl-a and the remote sensing reflectance, both of which could vary according to cell size [46,67]; and (iv) the optical depth [43,50], an aspect that could be explored in future works.

Finally, the higher uncertainties associated with the microplankton satellite estimates obtained in this and previous studies, which use the same PSC model, represent a limitation in the application of this model. However, there are at least two aspects that support the application of such a model in our case. The first one is that the satellite-derived spatial distribution of the PSC in CZ and CTZ in the study region is consistent with previous reports using in situ data from the same region; that is, nanoplankton dominates in the CTZ, whereas microplankton does so in the CZ, e.g., [30,60,81,84]. The second one is that previous in situ studies on PSC associated with mesoscale eddies have shown that an important fraction of the coastal microplankton in this region appears to be advected by these features during their early stages of development [32,33].

### *4.2. Shifts on Phytoplankton Size Classes within Mesoscale Eddies*

The main features of eddies, mean seaward speed (~2.5 km $d^{-1}$) and diameter (~80–120 km), are in agreement with previous reports for mid-latitude eddies (62–128 km) [7,19] and for eddies off central-southern Chile (~1–2 km $d^{-1}$ and 70–110 km) [30,32]. Regarding the PSC, the highest contributions of the microplankton fraction during the first 5 to 10 weeks of tracking ssAC1 and sC eddies are associated with their closer proximity to the CZ, characterized by upwelling waters rich in nutrients and in situ high microplankton abundance and Chl-a concentrations [84]. During this first period, the microplankton contribution inside these eddies was higher (about 0.2 difference) in comparison with the surrounding waters in the CZ. This difference could be a response to trapping and stirring of coastal waters within the eddies and/or by the vertical displacement of the isopycnals during eddy formation promoting an influx of nutrients and high phytoplankton productivity rates [10,11,14]. The shift of the phytoplankton community structure towards smaller PSC when the eddies were transiting through the CTZ is in agreement with in situ measurements off central-southern Chile, which indicated that similar eddy types were mostly dominated by smaller cells in the CTZ [32]. In the case of sAC and ssAC2, similar or lower microplankton fraction values were found in comparison with those in the CZ during the first weeks of tracking. For sAC, this could be explained as a response to the physical dynamics of this eddy type, usually characterized by a downward displacement of isopycnals, which forces a flush of nutrients below the euphotic zone and the consequent decrease in primary production [3,9–11]. In the case of ssAC2, Morales et al. [33] have previously described that this eddy was interacting with a coastal front during a relaxation phase of upwelling, time at which the nanoplankton made the largest contributions to total Chl-a.

The observed tendency of the PSC contributions throughout the complete follow-up period of eddies might be explained by factors such as changes in nutrient availability and grazing pressure. In the region off central-southern Chile, waters with high nitrate and silicate concentrations (~10 μM) have been associated with the upwelling of the Equatorial Subsurface Waters (ESSW) in the CZ, favoring the dominance of the microplankton fraction (e.g., diatoms) [85,86]. In contrast, waters in the CTZ are often lower in silicate concentration leading to changes in the nitrate:silicate ratios [33]. Ratios close to 1:1 have favored the growth of large phytoplankton cells, whilst higher values (>3:1) can produce shifts in the size of diatoms and/or changes towards other small functional groups [33,87,88]. Phytoplankton communities within eddies can also change as a result of predator-prey interactions. Paterson et al. [89] found a lack of phytoplankton biomass accumulation within a surface anticyclone eddy, which was attributed to zooplankton grazing, mostly upon diatoms. They also reported a higher zooplankton biomass inside this type of eddy compared with surface cyclonic eddy. In the region of study, however, it was not possible to test this aspect. Other processes, such as wind-eddy interactions, could favor the transport of phytoplankton below the euphotic zone [11], together with a faster sinking of microplankton cells when the nutrients are depleted [4], which can also generate shifts in the PSC within mesoscale eddies. Future work could be done complementing the three-component

model parameters here calculated together with regional biogeochemical models to better assess the changes of the phytoplankton community structure associated with the mesoscale features off central-southern Chile.

## 5. Conclusions

A three-component (micro-, nano-, and picoplankton) model for phytoplankton was tuned with in situ Chl-a data from surface waters in CZ and CTZ off central-southern Chile in order to retrieve the satellite estimates of PSC in this highly productive coastal upwelling region. The model was found to capture the trend of in situ SFF Chl-a measurements, and the model assumptions were met. The retrieved model PSC estimates showed the best agreement in the case of the nanoplankton and the combined nano- and picoplankton groups. In contrast, moderate to high uncertainties were found in the case of micro- and picoplankton, in concordance with a higher data dispersion of the picoplankton Chl-a measurements, making it difficult to fit accurate model parameters. The application of the estimated model parameters to total Chl-a satellite data show the best agreement between the satellite estimates of smaller PSC and in situ data measurements. However, the microplankton fraction displayed the highest uncertainty value, which was mainly associated with a larger data dispersion of satellite estimates for this fraction when total Chl-a values were low. Our results show a shift of the PSC from larger to smaller phytoplankton cells in the seaward transit of eddies, changes which appear to be associated with the location of the eddies with regard to the coast, eddy type, nutrient availability, and/or zooplankton grazing upon phytoplankton cells.

**Author Contributions:** In situ size-fractionated Chl-a data collection: C.E.M., V.A., and A.C.A. Parameterization of the three-component model for the study region: R.J.W.B. and A.C.A. Detection and tracking of eddies: P.A.A. Procedures and data analysis: C.E.M., O.P., S.H., and A.C.A. Manuscript writing: A.C.A. with input from all co-authors.

**Funding:** This research was funded by FONDECYT Project 1151299 (CONICYT-Chile) to C.E.M. and S.H. Additional support during the writing phase was provided by the Instituto Milenio de Oceanografía (IMO-Chile), funded by the Iniciativa Científica Milenio (ICM-Chile). A.C.A. was supported by a CONICYT-Chile Scholarship (2013–2017).

**Acknowledgments:** The authors thank the European Space Agency for the production and distribution of the Ocean Colour Climate Change Initiative dataset, Version 3.0, available online at http://www.esa-oceancolour-cci.org/. Sea level anomaly data were generated by DUACS and distributed by AVISO (ftp://ftp.aviso.oceanobs.com). Cross-Calibrated Multi-Platform (CCMP) Version-2.0 surface wind data were produced by Remote Sensing Systems, and are available at http://www.remss.com. We are grateful to the COPAS Center for providing total and size-fractionated Chl-a in situ data from St. 18 time series, and to FIP (Fondo de Investigación Pesquera) projects for providing total and size-fractionated Chl-a in situ data from the area off central-southern Chile (N°2004-20, N°2005-01, N°2006-12, N°2007-10, N°2008-20, N°2009-39 and N°2014-04-2).

**Conflicts of Interest:** The authors declare no conflict of interest.

## Appendix A

*Removal of Chlorophyll-a Variability Other than the Mesoscale*

In order to remove unwanted small and large-scale features unrelated to mesoscale variability of the size-fractionated Chl-a concentrations, the following procedure was carried out.

Step1: The monthly climatology was linearly interpolated to daily values. For this purpose, the monthly averages were centered on the 15th day of each month (e.g., $MA_{m1}$ and $MA_{m2}$); then, the interpolated monthly average for a specific day ($MA_d$) is given by the relationship:

$$MA_d = MA_{m1} \times W_1 + MA_{m2} \times W_2 \quad (4)$$

in which $W_1$ and $W_2$ represent the percentage contribution of each monthly average to the date of interest (i.e., $W_1$ will be 100% if the date of interest corresponds to the 15th of month 1).

Step 2: The daily interpolated climatology was subtracted from the daily size-fractionated Chl-a time series.

Step 3: An eight-day composite of the satellite dataset resulting from the previous step is calculated in $\log_{10}$ space.

Step 4: The spatial median of the whole study region (a box of ~800 km × 800 km; 32–39°S and 72–81°W) is estimated and removed at each time.

## Appendix B

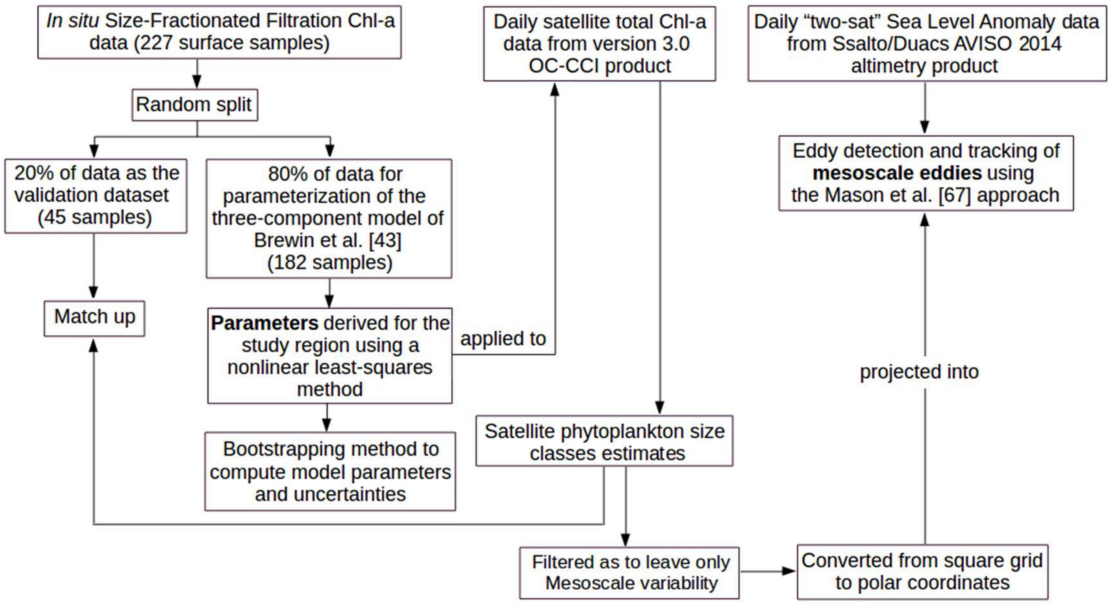


**Figure A1.** Flow-Diagram of the Methodological Procedures Used in This Study.

## Appendix C

**Table A1.** Symbols and Abbreviations.

| **Phytoplankton Size-Class Model** | |
|---|---|
| PSC | Phytoplankton size classes |
| $C$ | Total chlorophyll-a concentration |
| $C_M$ | Chlorophyll-a concentration by the micro-phytoplankton (>20 μm) |
| $C_N$ | Chlorophyll-a concentration by the nano-phytoplankton (2–20 μm) |
| $C_P$ | Chlorophyll-a concentration by the pico-phytoplankton (<2 μm) |
| $C_{NP}$ | Chlorophyll-a concentration by the combined nano- and pico-phytoplankton |
| $C_{NP}{}^m$ | Asymptotic maximum value of $C_{NP}$ |
| $C_P{}^m$ | Asymptotic maximum value of $C_P$ |
| $D_{NP}$ | Fraction contribution by the combined nano- and pico-phytoplankton to total chlorophyll-a as total tends to zero |
| $D_P$ | Fraction contribution by the pico-phytoplankton to total chlorophyll-a as total tends to zero |
| $F_M$ | Fraction of total chlorophyll-a for micro-phytoplankton |
| $F_N$ | Fraction of total chlorophyll-a for nano-phytoplankton |
| $F_P$ | Fraction of total chlorophyll-a for pico-phytoplankton |
| $F_{NP}$ | Fraction of total chlorophyll-a for the combined nano- and pico-phytoplankton |

**Table A1.** *Cont.*

| | |
|---|---|
| **In situ methods to characterize the phytoplankton size-classes** | |
| SFF | Size-fractionated filtration |
| $a_{ph}$ | Phytoplankton absorption spectra |
| HPLC | High performance liquid chromatography |
| **Statistical metrics** | |
| r | Pearson linear correlation coefficient |
| RMS | Root mean square error |
| MAE | Mean absolute error |
| MdAE | Median absolute error |
| δ | Bias |
| **Regional abbreviations** | |
| EBCS | Eastern Boundary Current Systems |
| CZ | Coastal zone |
| CTZ | Coastal transition zone |
| EA | Eastern Atlantic |
| SCS | Southern China Sea |
| AO | Atlantic Ocean |
| NEA | North-East Atlantic |
| NA | North Atlantic |
| CSC | Central-Southern Chile |
| **Mesoscale features (eddies)** | |
| sC | Surface cyclone |
| ssAC | Subsurface anticyclone |
| sAC | Surface anticyclone |
| ITE | Intrathermocline eddy |
| R | Eddy radius |
| r/R | A distance r from eddy center projected to eddy radius |
| SLA | Sea level anomaly |
| SSH | Sea surface height |

## References


1. Mann, K.H.; Lazier, J.R. *Dynamics of Marine Ecosystem*; Blakwell Sci.: Michigan, MI, USA, 1991; ISBN 0-86542-082-3.
2. Claustre, H.; Kerhervé, P.; Marty, J.C.; Prieur, L. Phytoplankton photoadaptation related to some frontal physical processes. *J. Mar. Syst.* **1994**, *5*, 251–265. [CrossRef]
3. Cotti-Rausch, B.E.; Lomas, M.W.; Lachenmyer, E.M.; Goldman, E.A.; Bell, D.W.; Goldberg, S.R. , Richardson, T.L. Mesoscale and sub-mesoscale variability in phytoplankton community composition in the Sargasso Sea. *Deep-Sea Res. I* **2016**, *110*, 106–122. [CrossRef]
4. McGillicuddy, D.J., Jr. Mechanisms of physical-biological-biogeochemical interaction at the oceanic mesoscale. *Annu. Rev. Mar. Sci.* **2016**, *8*, 125–159. [CrossRef] [PubMed]
5. Garçon, V.C.; Oschlies, A.; Doney, S.C.; McGillicuddy, D.J., Jr.; Waniek, J. The role of mesoscale variability on plankton dynamics in the North Atlantic. *Deep-Sea Res. II* **2001**, *48*, 2199–2226. [CrossRef]
6. McGillicuddy, D.J.; Anderson, L.A.; Bates, N.R.; Bibby, T.; Buesseler, K.O.; Carlson, C.A.; Davis, C.S.; Ewart, C.; Falkowski, P.G.; Goldthwait, S.A.; et al. Eddy/wind interactions stimulate extraordinary mid-ocean plankton blooms. *Science* **2007**, *316*, 1021–1026. [CrossRef] [PubMed]
7. Chaigneau, A.; Eldin, G.; Dewitte, B. Eddy activity in the four major upwelling systems from satellite altimetry (1992–2007). *Prog. Oceanogr.* **2009**, *83*, 117–123. [CrossRef]
8. He, Q.; Zhan, H.; Cai, S.; Zha, G. On the asymmetry of eddy-induced surface chlorophyll anomalies in the southeastern Pacific: The role of eddy-Ekman pumping. *Prog. Oceanogr.* **2016**, *141*, 202–211. [CrossRef]

9. McGillicuddy, D.J., Jr.; Robinson, A.R.; Siegel, D.A.; Jannasch, H.W.; Johnson, R.; Dickey, T.D.; McNeil, J.; Michaels, A.F.; Knap, A.H. Influence of mesoscale eddies on new production in the Sargasso Sea. *Nature* **1998**, *394*, 263–266. [CrossRef]
10. Sweeney, E.N.; McGillicuddy, D.J., Jr.; Buesseler, K.O. Biogeochemical impacts due to mesoscale eddy activity in the Sargasso Sea as measured at the Bermuda Atlantic Time-series Study (BATS). *Deep-Sea Res. II* **2003**, *50*, 3017–3039. [CrossRef]
11. Gaube, P.; McGillicuddy, D.J.; Chelton, D.B.; Behrenfeld, M.J.; Strutton, P.G. Regional variations in the influence of mesoscale eddies on near-surface chlorophyll. *J. Geophys. Res. Oceans* **2014**, *119*, 8195–8220. [CrossRef]
12. Wang, L.; Huang, B.; Chiang, K.P.; Liu, X.; Chen, B.; Xie, Y.; Xu, Y.; Hu, J.; Dai, M. Physical-biological coupling in the western South China Sea: The response of phytoplankton community to a mesoscale cyclonic eddy. *PLoS ONE* **2016**, *11*, e0153735. [CrossRef] [PubMed]
13. Combes, V.; Hormazabal, S.; Di Lorenzo, E. Interannual variability of the subsurface eddy field in the Southeast Pacific. *J. Geophys. Res. Oceans* **2015**, *120*, 4907–4924. [CrossRef]
14. Mourino-Carballido, B.; McGillicuddy, D.J. Mesoscale variability in the metabolic balance of the Sargasso Sea. *Limnol. Oceanogr.* **2006**, *51*, 2675–2689. [CrossRef]
15. Hormazabal, S.; Combes, V.; Morales, C.E.; Correa-Ramirez, M.A.; Di Lorenzo, E.; Nuñez, S. Intrathermocline eddies in the coastal transition zone off central Chile (31–41 S). *J. Geophys. Res. Oceans* **2013**, *118*, 4811–4821. [CrossRef]
16. Pegliasco, C.; Chaigneau, A.; Morrow, R. Main eddy vertical structures observed in the four major Eastern Boundary Upwelling Systems. *J. Geophys. Res. Oceans* **2015**, *120*, 6008–6033. [CrossRef]
17. Barceló-Llull, B.; Sangrà, P.; Pallàs-Sanz, E.; Barton, E.D.; Estrada-Allis, S.N.; Martínez-Marrero, A.; Marrero-Díaz, Á. Anatomy of a subtropical intrathermocline eddy. *Deep-Sea Res. I* **2017**, *124*, 126–139. [CrossRef]
18. Siegel, D.A.; Peterson, P.; McGillicuddy, D.J.; Maritorena, S.; Nelson, N.B. Bio-optical footprints created by mesoscale eddies in the Sargasso Sea. *Geophys. Res. Lett.* **2011**, *38*. [CrossRef]
19. Chelton, D.B.; Gaube, P.; Schlax, M.G.; Early, J.J.; Samelson, R.M. The influence of nonlinear mesoscale eddies on near-surface oceanic chlorophyll. *Science* **2011**, *334*, 328–332. [CrossRef] [PubMed]
20. Klein, P.; Lapeyre, G. The oceanic vertical pump induced by mesoscale and submesoscale turbulence. *Annu. Rev. Mar. Sci.* **2009**, *1*, 351–375. [CrossRef] [PubMed]
21. Martin, A.P.; Richards, K.J. Mechanisms for vertical nutrient transport within a North Atlantic mesoscale eddy. *Deep-Sea Res. II* **2001**, *48*, 757–773. [CrossRef]
22. Gaube, P.; Chelton, D.B.; Strutton, P.G.; Behrenfeld, M.J. Satellite observations of chlorophyll, phytoplankton biomass, and Ekman pumping in nonlinear mesoscale eddies. *J. Geophys. Res. Oceans* **2013**, *118*, 6349–6370. [CrossRef]
23. Gaube, P.; Chelton, D.B.; Samelson, R.M.; Schlax, M.G.; O'Neill, L.W. Satellite observations of mesoscale eddy-induced Ekman pumping. *J. Phys. Oceanogr.* **2015**, *45*, 104–132. [CrossRef]
24. Fielding, S.; Crisp, N.; Allen, J.T.; Hartman, M.C.; Rabe, B.; Roe, H.S.J. Mesoscale subduction at the Almeria–Oran front: Part 2. Biophysical interactions. *J. Mar. Syst.* **2001**, *30*, 287–304. [CrossRef]
25. Mahadevan, A.; Tandon, A. An analysis of mechanisms for submesoscale vertical motion at ocean fronts. *Ocean Model.* **2006**, *14*, 241–256. [CrossRef]
26. Nagai, T.; Tandon, A.; Gruber, N.; McWilliams, J.C. Biological and physical impacts of ageostrophic frontal circulations driven by confluent flow and vertical mixing. *Dyn. Atmos. Oceans* **2008**, *45*, 229–251. [CrossRef]
27. Omand, M.M.; D'Asaro, E.A.; Lee, C.M.; Perry, M.J.; Briggs, N.; Cetinić, I.; Mahadevan, A. Eddy-driven subduction exports particulate organic carbon from the spring bloom. *Science* **2015**, *348*, 222–225. [CrossRef] [PubMed]
28. Arístegui, J.; Barton, E.D.; Tett, P.; Montero, M.F.; García-Muñoz, M.; Basterretxea, G.; de Armas, D. Variability in plankton community structure, metabolism, and vertical carbon fluxes along an upwelling filament (Cape Juby, NW Africa). *Prog. Oceanogr.* **2004**, *62*, 95–113. [CrossRef]
29. Pelegrí, J.L.; Arístegui, J.; Cana, L.; González-Dávila, M.; Hernández-Guerra, A.; Hernández-León, S.; Santana-Casiano, M. Coupling between the open ocean and the coastal upwelling region off northwest Africa: Water recirculation and offshore pumping of organic matter. *J. Mar. Syst.* **2005**, *54*, 3–37. [CrossRef]

30. Correa-Ramirez, M.A.; Hormazabal, S.; Yuras, G. Mesoscale eddies and high chlorophyll concentrations off central Chile (29–39 S). *Geophys. Res. Lett.* **2007**, *34*. [CrossRef]
31. Gruber, N.; Lachkar, Z.; Frenzel, H.; Marchesiello, P.; Münnich, M.; McWilliams, J.C.; Plattner, G.K. Eddy-induced reduction of biological production in eastern boundary upwelling systems. *Nat. Geosci.* **2011**, *4*, 787–792. [CrossRef]
32. Morales, C.E.; Hormazabal, S.; Correa-Ramirez, M.; Pizarro, O.; Silva, N.; Fernandez, C.; Torreblanca, M.L. Mesoscale variability and nutrient–phytoplankton distributions off central-southern Chile during the upwelling season: The influence of mesoscale eddies. *Prog. Oceanogr.* **2012**, *104*, 17–29. [CrossRef]
33. Morales, C.E.; Anabalón, V.; Bento, J.P.; Hormazabal, S.; Cornejo, M.; Correa-Ramírez, M.A.; Silva, N. Front-Eddy Influence on Water Column Properties, Phytoplankton Community Structure, and Cross-Shelf Exchange of Diatom Taxa in the Shelf-Slope Area off Concepción (∼36–37°S). *J. Geophys. Res. Oceans* **2017**, *122*, 8944–8965. [CrossRef]
34. Moore II, T.S.; Matear, R.J.; Marra, J.; Clementson, L. Phytoplankton variability off the Western Australian Coast: Mesoscale eddies and their role in cross-shelf exchange. *Deep-Sea Res. II* **2007**, *54*, 943–960. [CrossRef]
35. Karrasch, B.; Hoppe, H.G.; Ullrich, S.; Podewski, S. The role of mesoscale hydrography on microbial dynamics in the northeast Atlantic: Results of a spring bloom experiment. *J. Mar. Res.* **1996**, *54*, 99–122. [CrossRef]
36. Ciotti, A.M.; Lewis, M.R.; Cullen, J.J. Assessment of the relationships between dominant cell size in natural phytoplankton communities and the spectral shape of the absorption coefficient. *Limnol. Oceanogr.* **2002**, *47*, 404–417. [CrossRef]
37. Guidi, L.; Stemmann, L.; Jackson, G.A.; Ibanez, F.; Claustre, H.; Legendre, L.; Gorskya, G. Effects of phytoplankton community on production, size, and export of large aggregates: A world-ocean analysis. *Limnol. Oceanogr.* **2009**, *54*, 1951–1963. [CrossRef]
38. Finkel, Z.V.; Beardall, J.; Flynn, K.J.; Quigg, A.; Rees, T.A.V.; Raven, J.A. Phytoplankton in a changing world: Cell size and elemental stoichiometry. *J. Plankton Res.* **2009**, *32*, 119–137. [CrossRef]
39. Ward, B.A.; Dutkiewicz, S.; Jahn, O.; Follows, M.J. A size-structured food-web model for the global ocean. *Limnol. Oceanogr.* **2012**, *57*, 1877–1891. [CrossRef]
40. Marañón, E. Cell size as a key determinant of phytoplankton metabolism and community structure. *Ann. Rev. Mar. Sci.* **2015**, *7*, 241–264. [CrossRef] [PubMed]
41. Brewin, R.J.; Sathyendranath, S.; Jackson, T.; Barlow, R.; Brotas, V.; Airs, R.; Lamont, T. Influence of light in the mixed-layer on the parameters of a three-component model of phytoplankton size class. *Remote Sens. Environ.* **2015**, *168*, 437–450. [CrossRef]
42. Uitz, J.U.; Huot, Y.; Bruyant, F.; Babin, M.; Claustre, H. Relating phytoplankton photophysiological properties to community structure on large scales. *Limnol. Oceanogr.* **2008**, *53*, 614–630. [CrossRef]
43. Brewin, R.J.; Sathyendranath, S.; Hirata, T.; Lavender, S.J.; Barciela, R.M.; Hardman-Mountford, N.J. A three-component model of phytoplankton size class for the Atlantic Ocean. *Ecol. Model.* **2012**, *221*, 1472–1483. [CrossRef]
44. Brewin, R.J.; Sathyendranath, S.; Tilstone, G.; Lange, P.K.; Platt, T. A multicomponent model of phytoplankton size structure. *J. Geophys. Res. Oceans* **2014**, *119*, 3478–3496. [CrossRef]
45. Brewin, R.J.; Sathyendranath, S.; Lange, P.K.; Tilstone, G. Comparison of two methods to derive the size-structure of natural populations of phytoplankton. *Deep-Sea Res. I* **2014**, *85*, 72–79. [CrossRef]
46. Ward, B.A. Temperature-correlated changes in phytoplankton community structure are restricted to polar waters. *PLoS ONE* **2015**, *10*, e0135581. [CrossRef] [PubMed]
47. Uitz, J.; Claustre, H.; Morel, A.; Hooker, S.B. Vertical distribution of phytoplankton communities in open ocean: An assessment based on surface chlorophyll. *J. Geophys. Res. Oceans* **2006**, *111*. [CrossRef]
48. Brewin, R.J.; Ciavatta, S.; Sathyendranath, S.; Jackson, T.; Tilstone, G.; Curran, K.; Airs, R.L.; Cummings, D.; Brotas, V.; Organelli, E.; et al. Uncertainty in ocean-color estimates of chlorophyll for phytoplankton groups. *Front. Mar. Sci.* **2017**, *4*, 104. [CrossRef]
49. Ciotti, A.M.; Bricaud, A. Retrievals of a size parameter for phytoplankton and spectral light absorption by colored detrital matter from water-leaving radiances at SeaWiFS channels in a continental shelf region off Brazil. *Limnol. Oceanogr. Methods* **2006**, *4*, 237–253. [CrossRef]

50. Brotas, V.; Brewin, R.J.; Sá, C.; Brito, A.C.; Silva, A.; Mendes, C.R.; Diniz, T.; Kaufmann, M.; Tarran, G.; Groom, S.B.; et al. Deriving phytoplankton size classes from satellite data: Validation along a trophic gradient in the eastern Atlantic Ocean. *Remote Sens. Environ.* **2013**, *134*, 66–77. [CrossRef]
51. Brito, A.C.; Sá, C.; Brotas, V.; Brewin, R.J.; Silva, T.; Vitorino, J.; Platt, T.; Sathyendranath, S. Effect of phytoplankton size classes on bio-optical properties of phytoplankton in the Western Iberian coast: Application of models. *Remote Sens. Environ.* **2015**, *156*, 537–550. [CrossRef]
52. Lin, J.; Cao, W.; Wang, G.; Hu, S. Satellite-observed variability of phytoplankton size classes associated with a cold eddy in the South China Sea. *Mar. Pollut. Bull.* **2014**, *83*, 190–197. [CrossRef] [PubMed]
53. Cáceres, M.M. Vórtices y filamentos observados en imágenes de satélite frente al área de surgencia de Talcahuano, Chile central. *Investig. Pesq.* **1992**, *37*, 55–66.
54. Shaffer, G.; Hormazabal, S.; Pizarro, O.; Salinas, S. Seasonal and interannual variability of currents and temperature off central Chile. *J. Geophys. Res. Oceans* **1999**, *104*, 29951–29961. [CrossRef]
55. Sobarzo, M.; Bravo, L.; Donoso, D.; Garcés-Vargas, J.; Schneider, W. Coastal upwelling and seasonal cycles that influence the water column over the continental shelf off central Chile. *Prog. Oceanogr.* **2007**, *75*, 363–382. [CrossRef]
56. Letelier, J.; Pizarro, O.; Nuñez, S. Seasonal variability of coastal upwelling and the upwelling front off central Chile. *J. Geophys. Res. Oceans* **2009**, *114*. [CrossRef]
57. Correa-Ramirez, M.A.; Hormazabal, S.; Morales, C.E. Spatial patterns of annual and interannual surface chlorophyll-a variability in the Peru–Chile Current System. *Prog. Oceanogr.* **2012**, *92*, 8–17. [CrossRef]
58. Morales, C.E.; Hormazabal, S.; Andrade, I.; Correa-Ramirez, M.A. Time-space variability of chlorophyll-a and associated physical variables within the region off Central-Southern Chile. *Remote Sens.* **2013**, *5*, 5550–5571. [CrossRef]
59. Hormazabal, S.; Shaffer, G.; Leth, O. Coastal transition zone off Chile. *J. Geophys. Res. Oceans* **2004**, *109*. [CrossRef]
60. Morales, C.E.; Anabalón, V. Phytoplankton biomass and microbial abundances during the spring upwelling season in the coastal area off Concepción, central-southern Chile: Variability around a time series station. *Prog. Oceanogr.* **2012**, *92*, 81–91. [CrossRef]
61. Fondo de Investigación Pesquera. *Fase II: Levantamiento Oceanográfico para Elaborar la Línea Base de los Montes Submarinos Juan Fernández 5 (JF5), Juan Fernández 6 (JF6) y Monte O'Higgins*; Informe final Proyecto FIP 2014-04-2; Chile, 2016; 355p, Available online: www.subpesca.cl/fipa/613/articles-92055_informe_final.pdf (accessed on 25 May 2018).
62. Sathyendranath, S.; Cota, G.; Stuart, V.; Maass, H.; Platt, T. Remote sensing of phytoplankton pigments: A comparison of empirical and theoretical approaches. *Int. J. Remote Sens.* **2001**, *22*, 249–273. [CrossRef]
63. Devred, E.; Sathyendranath, S.; Stuart, V.; Maass, H.; Ulloa, O.; Platt, T. A two-component model of phytoplankton absorption in the open ocean: Theory and applications. *J. Geophys. Res. Oceans* **2006**, *111*, C03011. [CrossRef]
64. Vidussi, F.; Claustre, H.; Manca, B.B.; Luchetta, A.; Marty, J.C. Phytoplankton pigment distribution in relation to upper thermocline circulation in the eastern Mediterranean Sea during winter. *J. Geophys. Res. Oceans* **2001**, *106*, 19939–19956. [CrossRef]
65. Efron, B. Bootstrap methods: Another look at the jackknife annals of statistics. *Ann. Stat.* **1979**, *7*, 1–26. [CrossRef]
66. Bailey, S.W.; Werdell, P.J. A multi-sensor approach for the on-orbit validation of ocean color satellite data products. *Remote Sens. Environ.* **2006**, *102*, 12–23. [CrossRef]
67. Seegers, B.N.; Stumpf, R.P.; Schaeffer, B.A.; Loftin, K.A.; Werdell, P.J. Performance metrics for the assessment of satellite data products: An ocean color case study. *Opt. Express* **2018**, *26*, 7404–7422. [CrossRef] [PubMed]
68. Mason, E.; Pascual, A.; McWilliams, J.C. A new sea surface height–based code for oceanic mesoscale eddy tracking. *J. Atmos. Ocean. Technol.* **2014**, *31*, 1181–1188. [CrossRef]
69. Kurian, J.; Colas, F.; Capet, X.; McWilliams, J.C.; Chelton, D.B. Eddy properties in the California current system. *J. Geophys. Res. Oceans* **2011**, *116*, C08027. [CrossRef]
70. Penven, P.; Echevin, V.; Pasapera, J.; Colas, F.; Tam, J. Average circulation, seasonal cycle, and mesoscale dynamics of the Peru Current System: A modeling approach. *J. Geophys. Res. Oceans* **2005**, *110*. [CrossRef]

71. Capet, A.; Mason, E.; Rossi, V.; Troupin, C.; Faugere, Y.; Pujol, I.; Pascual, A. Implications of refined altimetry on estimates of mesoscale activity and eddy-driven offshore transport in the Eastern Boundary Upwelling Systems. *Geophys. Res. Lett.* **2014**, *41*, 7602–7610. [CrossRef]
72. Campbell, J.W. The lognormal distribution as a model for bio-optical variability in the sea. *J. Geophys. Res. Oceans* **1995**, *100*, 13237–13254. [CrossRef]
73. Dufois, F.; Hardman-Mountford, N.J.; Greenwood, J.; Richardson, A.J.; Feng, M.; Matear, R.J. Anticyclonic eddies are more productive than cyclonic eddies in subtropical gyres because of winter mixing. *Sci. Adv.* **2016**, *2*, e1600282. [CrossRef] [PubMed]
74. Gutiérrez, D.; Akester, M.; Naranjo, L. Productivity and sustainable management of the Humboldt Current large marine ecosystem under climate change. *Environ. Dev.* **2016**, *17*, 126–144. [CrossRef]
75. Lohrenz, S.; Weidemann, A.; Tuel, M. Phytoplankton spectral absorption as influenced by community size structure and pigment composition. *J. Plankton Res.* **2003**, *25*, 35–61. [CrossRef]
76. Baird, M.; Timko, P.; Wu, L. The effect of packaging of chlorophyll within phytoplankton and light scattering in a coupled physical-biological ocean model. *Mar. Freshw. Res.* **2007**, *58*, 966–981. [CrossRef]
77. Nair, A.; Sathyendranath, S.; Platt, T.; Morales, J.; Stuart, V.; Forget, M.H.; Devred, E.; Bouman, H. Remote sensing of phytoplankton functional types. *Remote Sens. Environ.* **2008**, *112*, 3366–3375. [CrossRef]
78. Hopcroft, R.R.; Roff, J.C. Phytoplankton size fractions in a tropical neritic ecosystem near Kingston, Jamaica. *J. Plankton Res.* **1990**, *12*, 1069–1088. [CrossRef]
79. Gin, K.Y.H.; Lin, X.; Zhang, S. Dynamics and size structure of phytoplankton in the coastal waters of Singapore. *J. Plankton Res.* **2000**, *22*, 1465–1484. [CrossRef]
80. Sathyendranath, S.; Platt, T. Spectral effects in bio-optical control on the ocean system. *Oceanologia* **2007**, *49*, 5–39.
81. Anabalón, V.; Morales, C.E.; Escribano, R.; Varas, M.A. The contribution of nano-and micro-planktonic assemblages in the surface layer (0–30 m) under different hydrographic conditions in the upwelling area off Concepción, central Chile. *Prog. Oceanogr.* **2007**, *75*, 396–414. [CrossRef]
82. González, H.E.; Menschel, E.; Aparicio, C.; Barría, C. Spatial and temporal variability of microplankton and detritus, and their export to the shelf sediments in the upwelling area off Concepción, Chile (∼36S), during 2002–2005. *Prog. Oceanogr.* **2007**, *75*, 435–451. [CrossRef]
83. Böttjer, D.; Morales, C.E. Nanoplanktonic assemblages in the upwelling area off Concepción (∼36°S), central Chile: Abundance, biomass, and grazing potential during the annual cycle. *Prog. Oceanogr.* **2007**, *75*, 415–434. [CrossRef]
84. Morales, C.E.; González, H.E.; Hormazabal, S.; Yuras, G.; Letelier, J.; Castro, L.R. The distribution of chlorophyll-a and dominant planktonic components in the coastal transition zone off Concepción, central Chile, during different oceanographic conditions. *Prog. Oceanogr.* **2007**, *75*, 452–469. [CrossRef]
85. Anabalón, V.; Morales, C.E.; González, H.E.; Menschel, E.; Schneider, W.; Hormazabal, S.; Escribano, R. Micro-phytoplankton community structure in the coastal upwelling zone off Concepción (central Chile): Annual and inter-annual fluctuations in a highly dynamic environment. *Prog. Oceanogr.* **2016**, *149*, 174–188. [CrossRef]
86. Llanillo, P.J.; Pelegrí, J.L.; Duarte, C.; Emelianov, M.; Gasser, M.; Gourrion, M.J.; Rodríguez-Santana, A. Meridional and zonal changes in water properties along the continental slope off central and northern Chile. *Cienc. Mar.* **2012**, *38*, 307–332. [CrossRef]
87. Harrison, P.J.; Davis, C.O. The use of outdoor phytoplankton continuous cultures to analyze factors influencing species succession. *J. Exp. Mar. Biol. Ecol.* **1979**, *41*, 9–23. [CrossRef]
88. Raven, J.A. Small is beautiful: The picophytoplankton. *Funct. Ecol.* **1998**, *12*, 503–513. [CrossRef]
89. Paterson, H.; Knott, B.; Waite, A. Microzooplankton community structure and grazing on phytoplankton, in an eddy pair in the Indian Ocean off Western Australia. *Deep-Sea Res. Part II* **2007**, *54*, 1076–1093. [CrossRef]